Engineering Analysis with Boundary Elements 94 (2018) 94–102

Contents lists available at ScienceDirect

Engineering Analysis with Boundary Elements

journal homepage: www.elsevier.com/locate/enganabound

Domain-decomposition generalized finite difference method for stress analysis in multi-layered elastic materials

Yuanyuan Wang [a], Yan Gu [a,*], Chia-Ming Fan [b], Wen Chen [c], Chuanzeng Zhang [d]

[a] School of Mathematics and Statistics, Qingdao University, Qingdao 266071, PR China
[b] Department of Harbor and River Engineering & Computation and Simulation Center, National Taiwan Ocean University, Keelung 20224, Taiwan
[c] College of Mechanics and Materials, Hohai University, Nanjing 210098, PR China
[d] Department of Civil Engineering, University of Siegen, Paul-Bonatz-Str. 9-11, D-57076 Siegen, Germany

ARTICLE INFO

Keywords:
Multi-layered materials
Meshless method
Generalized finite difference method
Domain decomposition technique
Elasticity

ABSTRACT

The generalized finite difference method (GFDM) is a relatively new meshless method for the numerical solution of certain boundary value problems. The method uses the Taylor series expansions and the moving least squares approximation to derive explicit formulae for the required partial derivatives of unknown variables. In this paper, we document the first attempt to apply the GFDM for the numerical solution of two-dimensional (2D) multi-layered elastic problems. A multi-domain GFDM scheme is proposed to model the composite (layered) elastic materials. The composite material considered is decomposed into several sub-domains and, in each sub-domain, the solution is approximated by using the GFDM-type expansion. On the subdomain interface, compatibility of displacements and equilibrium of tractions are imposed. Preliminary numerical experiments show that the introduced multi-domain GFDM is very promising for accurate and efficient numerical simulations of multi-layered materials.

1. Introduction

Following the rapid improvement of industrial technology, more and more new materials have been synthesized, designed and utilized in recent years. Among these materials, the multi-layered materials which contain single or multiple layers have been widely utilized in industrial application to improve machining performance [1–4]. The coating layers can protect the substrate material against adhesion diffusion and intensive abrasive wear, due to their better temperature and wear resistant properties. However, the rather complex and expensive experimental investigations on composite (layered) materials underlie a general lack of the analytical or numerical modeling efforts which can accurately and efficiently predict the performances of multi-layered coating structures [5–8].

The well-established and widely applied finite element method (FEM) offers without doubt many advantages in solving multi-layered problems due to its flexibilities in dealing with the geometry, loading type and nonlinearities of the coating layers. The FEM itself, however, has also many inherent shortcomings especially when a re-meshing is required or when the elements become highly distorted [9,10]. As an alternative numerical approach, the boundary element method (BEM) can be applied efficiently to avoid such shortcomings become of the boundary-only discretization and its semi-analytical nature. In the past two decades, the BEM has been rapidly improved and can be nowadays considered as a competing method to the FEM. As a price paid for such a merit, the classical BEM, however, has to compute various singular and/or nearly singular integrals over the boundary elements, which is usually a cumbersome and non-trivial task [11–17].

Over the past two decades, some considerable effort was devoted to circumventing the shortcomings associated with the classical FEM and BEM methods. This drives to the development of various meshless methods which require neither domain nor boundary meshing [18–20]. The meshless methods still require discretization via sets of boundary and/or domain nodes, but these nodes need not have any connectivity and the trial functions are built entirely in terms these scattered irregular clouds of nodes. For an overview of the state of the art, we refer the readers to Refs. [16,21–25], as well as the references therein.

The generalized finite difference method (GFDM) is a relatively new meshless method. The main idea of the method is to combine the Taylor series expansion and the moving-least squares (MLS) approximation to derive explicit formulae for the required partial derivatives of unknown variables. The derivatives of unknown variables, and then, can be approximated by a linear combination of function values with respect to its neighboring nodes. The key idea of the GFDM was proposed in the early eighties by Lizska and Orkisz [26,27] and were later essentially extended and improved by many other authors [28–37]. Prior to this study, this

* Corresponding author.
E-mail address: guyan1913@163.com (Y. Gu).

https://doi.org/10.1016/j.enganabound.2018.06.006
Received 14 April 2018; Received in revised form 10 June 2018; Accepted 10 June 2018
Available online 27 June 2018

method has been successfully tried for 2D and 3D parabolic and hyperbolic equations [30,38,39], third- and fourth-order partial differential equations [40], dynamic analysis of beams and plates [41], non-linear elliptic partial differential equations [42], and applied inverse problems [31,43,44]. In recent years, several other meshless methods have been considered and developed by researchers to obtain numerical solutions for different types of partial differential equations. The methods include, but are not limited to, the element-free Galerkin (EFG) method [45], the local radial point interpolation method (LRPIM) [46], the meshless local Petrov-Galerkin (MLPG) method [47], the boundary point interpolation method (BPIM) [48], the method of fundamental solutions (MFS) [49], and the singular boundary method (SBM) [25]. Each of the above-mentioned methods has its own merits and demerits. Interested readers are referred to excellent overview articles [24,25,45] on the development of this topic.

In this paper, we extend the GFDM to problems of stress analysis in multi-layered elastic materials. The multi-layered problems under consideration in this paper are solved using a non-overlapping domain decomposition method (DDM), in which the composite material is decomposed into several sub-domains and, in each sub-domain, the solution is approximated by using the GFDM-type expansion. On the subdomain interface, compatibility of displacements and equilibrium of tractions are imposed. These interface continuity conditions are satisfied in a least-squares sense in the same way as the boundary conditions of the problem. There are two main forms of the DDMs, which are the overlapping DDM and non-overlapping DDM. As compared to overlapping methods, the non-overlapping DDM has become very appalling for its inherent parallelism and flexibility. We refer to the papers [50,51] for theoretical and numerical results for non-overlapping DDM and to the references given there. In recent decades, the combination of the DDM and other methods has been proposed for the numerical solutions of elastic problems in layered materials. In Ref. [52], Berger and Karageorghis used the method of fundamental solutions (MFS) to deal with the stress analysis in layered elastic materials. In Ref. [53], Gu et al. applied the meshless singular boundary method (SBM) in conjunction with domain decomposition technique for the stress analysis of layered elastic materials. In Ref. [54], Yan et al. employed a local RBF collocation method for solving elastic waves in multi-layered functionally graded materials.

A brief outline of the rest of the paper is organized as follows. In Section 2, the GFDM formulation and its numerical implementation for the solution of general 2D elastic problems are briefly discussed. A multi-domain GFDM scheme for the solution of multi-layered elastic problems is presented in Section 3. In Section 4, three benchmark numerical examples are presented to validate the computational code and assess the performances of the proposed GFDM scheme. Finally, some conclusions and remarks are provided in Section 5.

2. The GFDM for isotropic problems in linear elasticity

2.1. Statement of the basic problem

The equilibrium equations for 2D problems in linear elasticity, in terms of the displacements, $u_i(\boldsymbol{x})$, $i=1, 2$, can be stated as [4]

$$\left\{2\frac{1-\mu}{1-2\mu}\right\}\frac{\partial^2 u_1(\boldsymbol{x})}{\partial x_1^2}+\frac{\partial^2 u_1(\boldsymbol{x})}{\partial x_2^2}+\left\{\frac{1}{1-2\mu}\right\}\frac{\partial^2 u_2(\boldsymbol{x})}{\partial x_1\partial x_2}=f_1(\boldsymbol{x}), \tag{1}$$

$$\left\{\frac{1}{1-2\mu}\right\}\frac{\partial^2 u_1(\boldsymbol{x})}{\partial x_1\partial x_2}+\frac{\partial^2 u_2(\boldsymbol{x})}{\partial x_1^2}+\left\{2\frac{1-\mu}{1-2\mu}\right\}\frac{\partial^2 u_2(\boldsymbol{x})}{\partial x_2^2}=f_2(\boldsymbol{x}), \tag{2}$$

subject to the boundary conditions

$$u_i(\boldsymbol{x})=\bar{u}_i(\boldsymbol{x}) \quad \boldsymbol{x}\in\Gamma_u \quad (\textit{Dirichlet boundary conditions}), \tag{3}$$

$$t_i(\boldsymbol{x})=\sigma_{ij}(\boldsymbol{x})n_j(\boldsymbol{x})=\bar{t}_i(\boldsymbol{x}) \quad \boldsymbol{x}\in\Gamma_t \quad (\textit{Neumann boundary conditions}), \tag{4}$$

where $\boldsymbol{x}=(x_1, x_2)$, μ is the Poisson's ratio, $t_i(\boldsymbol{x})$ denotes the component of boundary traction in the ith coordinate direction, $n_j(\boldsymbol{x})$ are the outward unit normal vector, Γ_u and Γ_t construct the whole boundary of the domain Ω, $\bar{u}_i$ and $\bar{t}_i$ represent the prescribed displacements and tractions, respectively, $f_1(\boldsymbol{x})$ and $f_2(\boldsymbol{x})$ in Eqs. (1) and (2) denote the inhomogeneous terms. Here and in the following, the customary Einstein's notation for summation over repeated subscripts is applied. The kinematics of deformation is described by the linear strain tensor

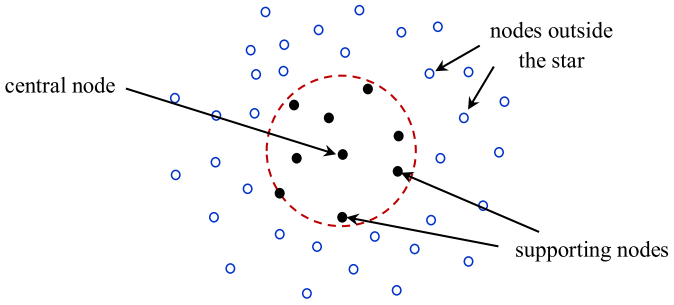

Fig. 1. An irregular cloud of points and the selection of stars in the GFDM.

$$\varepsilon_{ij}(\boldsymbol{x})=\frac{1}{2}\left\{\frac{\partial u_i(\boldsymbol{x})}{\partial x_j}+\frac{\partial u_j(\boldsymbol{x})}{\partial x_i}\right\}, \tag{5}$$

where sufficiently small displacements and displacement gradients are assumed. The stresses $\sigma_{ij}(\boldsymbol{x})$ are related to the strains $\varepsilon_{ij}(\boldsymbol{x})$ through generalized Hooke's law by

$$\sigma_{ij}(\boldsymbol{x})=2G\left(\varepsilon_{ij}(\boldsymbol{x})+\frac{\mu}{1-2\mu}\varepsilon_{kk}(\boldsymbol{x})\delta_{ij}\right), \tag{6}$$

where G stands for the shear modulus, δ_{ij} is the well-known Kronecker delta. The boundary tractions $t_i(\boldsymbol{x})$, $i=1, 2$, are defined in terms of the stresses as

$$t_i(\boldsymbol{x})=\sigma_{ij}(\boldsymbol{x})n_j(\boldsymbol{x}), \quad \boldsymbol{x}\in\Gamma. \tag{7}$$

Eqs. (1)–(7) completely describe the isotropic problems in linear elasticity.

2.2. Explicit formulae in GFDM

Without loss of generality, let us consider the following general differential equation in the 2D domain [42]

$$a_1\frac{\partial U}{\partial x_1}+a_2\frac{\partial U}{\partial x_2}+a_3\frac{\partial^2 U}{\partial x_1^2}+a_4\frac{\partial^2 U}{\partial x_2^2}+a_5\frac{\partial^2 U}{\partial x_1\partial x_2}=f(\boldsymbol{x}), \tag{8}$$

or for brevity

$$L_2[U]=f(\boldsymbol{x}), \tag{9}$$

where $L_2[U]$ is a second-order partial differential operator, $f(\boldsymbol{x})$ is known function, a_i, $i=1, 2, \ldots, 5$, are constants.

In order to obtain the explicit GFDM formulae for partial differential equations, an irregular cloud of points is scattered in the computational domain (see Fig. 1). For each given node $\boldsymbol{x}_0$, named as the central node, the m nearest nodes $\boldsymbol{x}_i$ ($i=1, 2, \ldots, m$), called the neighbors or supporting nodes, will be found within a prescribed distance d_m from the central node $\boldsymbol{x}_0$, i.e., $|\boldsymbol{x}_i-\boldsymbol{x}_0|\le d_m$. The concept of the '*star*' then refers to the area of all supporting nodes in relation to the central node [38]. Each node scattered inside the computational domain has an associated star assigned.

Suppose U_0 is the value of the function at the central node $\boldsymbol{x}_0$ and U_i, $i=1, 2, \ldots, m$, are function values at the rest of the nodes inside the star. Expanding the values of U_i around the central point $\boldsymbol{x}_0$ using the Taylor series expansion, we have [39,55]

$$U_i=U_0+h_i\frac{\partial U_0}{\partial x_1}+k_i\frac{\partial U_0}{\partial x_2}+\frac{h_i^2}{2}\frac{\partial^2 U_0}{\partial x_1^2}+\frac{k_i^2}{2}\frac{\partial^2 U_0}{\partial x_2^2}+h_ik_i\frac{\partial^2 U_0}{\partial x_1\partial x_2}+\ldots\ldots, \quad i=1, 2, \ldots, m. \tag{10}$$

Employing indicial notation for the coordinates of points $\boldsymbol{x}_0$ and $\boldsymbol{x}_i$, i.e., $\boldsymbol{x}_0 = (x_0^1, x_0^2)$ and $\boldsymbol{x}_i = (x_i^1, x_i^2)$, respectively, the coefficients in the Taylor series expansion (10) can be written as

$$h_i = x_i^1 - x_0^1, \quad k_i = x_i^2 - x_0^2. \tag{11}$$

When the Taylor series (10) is truncated after the second-order derivatives, it is then possible to define the following residual function $B(U)$

$$B(U) = \sum_{i=1}^{m} \left[\left(U_0 - U_i + h_i \frac{\partial U_0}{\partial x_1} + k_i \frac{\partial U_0}{\partial x_2} + \frac{h_i^2}{2} \frac{\partial^2 U_0}{\partial x_1^2} + \frac{k_i^2}{2} \frac{\partial^2 U_0}{\partial x_2^2} + h_i k_i \frac{\partial^2 U_0}{\partial x_1 \partial x_2} \right) \omega_i \right]^2, \tag{12}$$

where $\omega_i = \omega(h_i, k_i)$ denotes the weighting coefficients at point $\boldsymbol{x}_i$. In our computations, the weighting coefficients are taken to be

$$\omega_i = 1 - 6\left(\frac{d_i}{d_m}\right)^2 + 8\left(\frac{d_i}{d_m}\right)^3 - 3\left(\frac{d_i}{d_m}\right)^4, \quad d_i \le d_m. \tag{13}$$

where $d_i = \|\boldsymbol{x}_i - \boldsymbol{x}_0\|$ is the distance between points $\boldsymbol{x}_0$ and $\boldsymbol{x}_i$, d_m stands for the distance between nodes $\boldsymbol{x}_0$ and the farthest node inside the star. The weighting coefficients are inversely related to the distance from the corresponding node to the central node of the star, indicating that the Taylor series approximation is more important if the point $\boldsymbol{x}_i$ is closer to the central node $\boldsymbol{x}_0$. Of course other choices of weighting functions are possible, see Refs. [28,56].

Let, for brevity,

$$\boldsymbol{D}_U = \left\{ \frac{\partial U_0}{\partial x_1}, \frac{\partial U_0}{\partial x_2}, \frac{\partial^2 U_0}{\partial x_1^2}, \frac{\partial^2 U_0}{\partial x_2^2}, \frac{\partial^2 U_0}{\partial x_1 \partial x_2} \right\}^T, \tag{14}$$

$$\boldsymbol{p}_i = \left\{ h_i,\ k_i,\ h_i^2/2,\ k_i^2/2,\ h_i k_i \right\}, \quad i = 1, 2, \ldots m, \tag{15}$$

and

$$\boldsymbol{P} = \begin{bmatrix} \boldsymbol{p}_1 \\ \boldsymbol{p}_2 \\ \vdots \\ \boldsymbol{p}_m \end{bmatrix} = \begin{bmatrix} h_1 & k_1 & \cdots & h_1 k_1 \\ h_2 & k_2 & \cdots & h_2 k_2 \\ \vdots & \vdots & \ddots & \vdots \\ h_m & k_m & \cdots & h_m k_m \end{bmatrix}. \tag{16}$$

Then the residual function $B(U)$ defined in Eq. (12) can be expressed in the following matrix notation [42]

$$B(U) = \left(\boldsymbol{P}\boldsymbol{D}_U + \boldsymbol{U}_0 - \boldsymbol{U} \right)^T \boldsymbol{W} \left(\boldsymbol{P}\boldsymbol{D}_U + \boldsymbol{U}_0 - \boldsymbol{U} \right), \tag{17}$$

where $\boldsymbol{U} = \{U_1, U_2, \cdots, U_m\}^T$, $\boldsymbol{U}_0 = \{U_0, U_0, \cdots, U_0\}^T$ and $\boldsymbol{W} = diag(\omega_1^2, \omega_2^2, \cdots, \omega_m^2)$.

By minimizing the residual function $B(U)$ with respect to the partial derivatives $\boldsymbol{D}_U$, i.e.,

$$\frac{\partial B(U)}{\partial \{\boldsymbol{D}_U\}} = 0, \tag{18}$$

then the following linear equation system can be obtained (for each node of the discretization)

$$\boldsymbol{A}\boldsymbol{D}_U = \boldsymbol{b}, \tag{19}$$

where

$$\boldsymbol{A} = \begin{bmatrix} h_1 & k_1 & \cdots & h_1 k_1 \\ h_2 & k_2 & \cdots & h_2 k_2 \\ \vdots & \vdots & \ddots & \vdots \\ h_m & k_m & \cdots & h_m k_m \end{bmatrix}^T \begin{bmatrix} \omega_1^2 & & & \\ & \omega_2^2 & & \\ & & \ddots & \\ & & & \omega_m^2 \end{bmatrix} \begin{bmatrix} h_1 & k_1 & \cdots & h_1 k_1 \\ h_2 & k_2 & \cdots & h_2 k_2 \\ \vdots & \vdots & \ddots & \vdots \\ h_m & k_m & \cdots & h_m k_m \end{bmatrix} = \boldsymbol{P}^T \boldsymbol{W} \boldsymbol{P}, \tag{20}$$

and

$$\boldsymbol{b} = \boldsymbol{P}^T \boldsymbol{W} \left(\boldsymbol{U} - \boldsymbol{U}_0 \right). \tag{21}$$

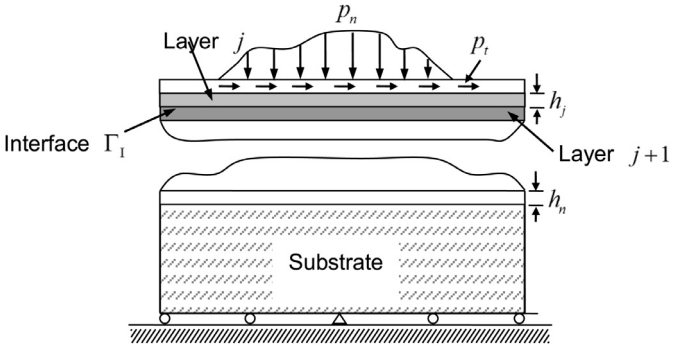

Fig. 2. Domain decomposition technique for the multi-coated elastic solids.

According to Eqs. (19)–(21), the partial derivative vector $\boldsymbol{D}_U$ as defined in Eq. (14) can now be expressed as, see Ref. [42]

$$\begin{aligned} \boldsymbol{D}_U &= \boldsymbol{A}^{-1}\boldsymbol{b} = \boldsymbol{A}^{-1}\boldsymbol{P}^T\boldsymbol{W}\left(\boldsymbol{U} - \boldsymbol{U}_0\right) \\ &= \boldsymbol{A}^{-1}\left(-\sum_{i=1}^{m} \omega_i^2 \boldsymbol{p}_i^T,\ \omega_1^2 \boldsymbol{p}_1^T,\ \ldots, \omega_m^2 \boldsymbol{p}_m^T \right) \begin{pmatrix} U_0 \\ U_1 \\ U_2 \\ \vdots \\ U_m \end{pmatrix}. \end{aligned} \tag{22}$$

For each node $\boldsymbol{x}_0$ inside the computational domain, the derivatives of the unknown function at $\boldsymbol{x}_0$ can now be approximated by a linear combination of function values at its neighboring nodes, as shown in Eq. (22). Substituting Eq. (22) into the governing Eq. (8) leads to

$$L_2[U_0] - f(\boldsymbol{x}) = m_0 U_0 + \sum_{i=1}^{m} m_i U_i - f(\boldsymbol{x}), \tag{23}$$

where the coefficients m_0 and m_i ($i = 1, 2, \ldots, m$) can be obtained from Eq. (22). Repeating the same procedure to each one of the nodes inside the computational domain, a system of linear algebraic equations can then be established. On solving this equation system, the numerical results of the function U at each node inside the domain can be obtained.

It is interesting to note that there exists several essential factors to influence the overall accuracy of the GFDM approximation, i.e.,

Factor 1: A suitable weighting function which will give more influence to the nodes closest to the central node;

Factor 2: The optimal number of nodes selected inside each of the stars (m);

Factor 3: An optimal criterion for the adaptive selection of nodes (the location of nodes) inside each of the stars.

A detailed review on advantages and drawbacks of different strategies for these factors is beyond the scope of the paper, and interested readers may find a detailed discussion on this subject in Refs. [30,38].

3. Non-overlapping domain-decomposition GFDM for multi-layered materials

One way to model the multi-layered materials is to use the non-overlapping DDM. The main idea behind this method is that the whole computational domain is broken up into separate sub-domains and the final system of equations is then formed by assembling algebraic equations written for each subdomain, based on the compatibility of displacements and equilibrium of tractions at the interface of the multi-layered materials. The main idea of this method is summarized hereafter, more details can be found in Refs. [53,57].

Fig. 2 shows an elastic body coated with n elastic layers. The boundary and interface conditions for each layer can be written as follows:

(1) Along every interface Γ_I between jth and $j+1$th layers, both displacements U and tractions T are unknowns. To solve the problem

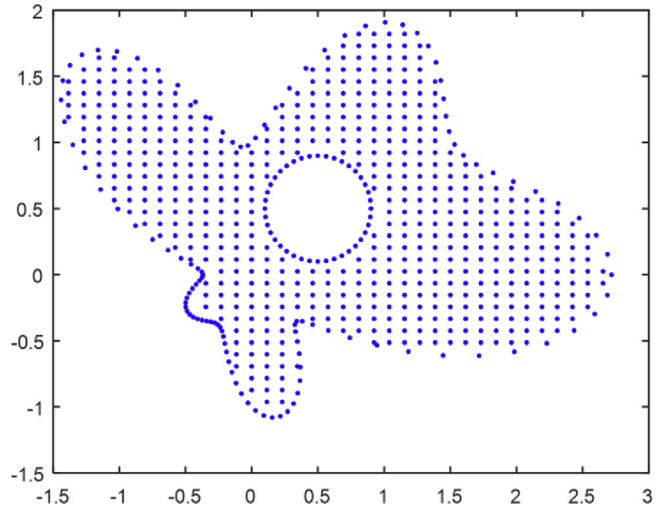

Fig. 3. Geometry of the problem and the configuration of the GFDM nodes.

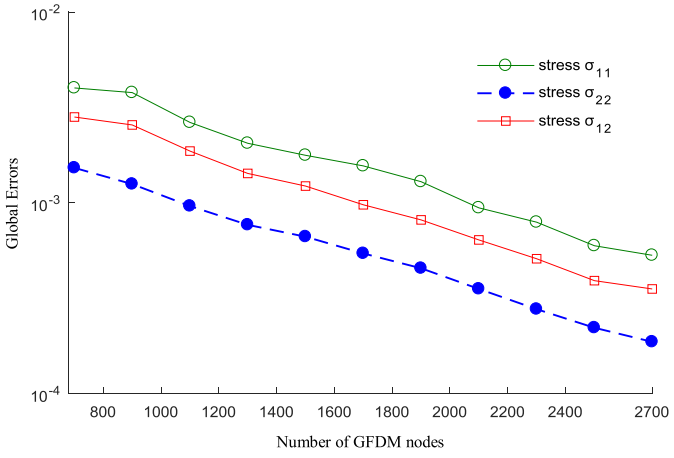

Fig. 4. Convergence curves of the calculated stresses at interior points inside the computational domain.

numerically, there will be the same number of algebraic equations as the unknowns. Therefore, the following continuity conditions at the interface must be considered:

$$T_{\mathrm{In}} = T_{\mathrm{In}}^{j} = -T_{\mathrm{In}}^{j+1}, \quad T_{\mathrm{It}} = T_{\mathrm{It}}^{j} = -T_{\mathrm{It}}^{j+1} \tag{24}$$

$$U_{\mathrm{In}} = U_{\mathrm{In}}^{j} = U_{\mathrm{In}}^{j+1}, \quad U_{\mathrm{It}} = U_{\mathrm{It}}^{j} = U_{\mathrm{It}}^{j+1} \tag{25}$$

where the subscript (In) indicates interface (I) and normal (n) component, and subscript (It) stands for interface (I) and tangential (t) direction.

(2) On the external surfaces (boundaries beside the interface Γ_{I}), the traction boundary conditions are given as:

$$T_n = p_n, \quad T_t = p_t \tag{26}$$

where T_n and T_t are the normal and tangential components of the traction, p_n and p_t the applied loads in the normal and tangential directions, respectively. In addition, the coating system is constrained, with specified displacement, at the bottom of the substrate.

Without loss of generality, the two layers j and $j+1$ with interface Γ_{I}, as illustrated in Fig. 2, are analyzed. In the jth layer, the solution can be approximated by the GFDM expansion as

$$\left[G^{j}\right]\begin{Bmatrix}\{u^{j}\}\\ \{u_{\mathrm{I}}^{j}\}\end{Bmatrix} = \{U^{j}\}, \quad \left[G_{\mathrm{I}}^{j}\right]\begin{Bmatrix}\{u^{j}\}\\ \{u_{\mathrm{I}}^{j}\}\end{Bmatrix} = \left\{U_{\mathrm{I}}^{j}\right\}, \tag{27}$$

$$\left[H^{j}\right]\begin{Bmatrix}\{u^{j}\}\\ \{u_{\mathrm{I}}^{j}\}\end{Bmatrix} = \{T^{j}\} \ , \ \left[H_{\mathrm{I}}^{j}\right]\begin{Bmatrix}\{u^{j}\}\\ \{u_{\mathrm{I}}^{j}\}\end{Bmatrix} = \left\{T_{I}^{j}\right\} \tag{28}$$

where U_{I}^{j}, T_{I}^{j} and u_{I}^{j} denote the interface displacements, tractions, and the unknown variables of layer j on the interface Γ_{I}, U^{j}, T^{j} and u^{j} the displacements, tractions, and the unknown variables of layer j on the remaining surfaces. G^{j}, G_{I}^{j}, H^{j}, and H_{I}^{j} are coefficient matrices of the GFDM expansion.

Similarly, for the $(j+1)$th layer, we have:

$$\left[G^{j+1}\right]\begin{Bmatrix}\{u^{j+1}\}\\ \{u_{\mathrm{I}}^{j+1}\}\end{Bmatrix} = \{U^{j+1}\} \ , \ \left[G_{\mathrm{I}}^{j+1}\right]\begin{Bmatrix}\{u^{j+1}\}\\ \{u_{\mathrm{I}}^{j+1}\}\end{Bmatrix} = \left\{U_{\mathrm{I}}^{j+1}\right\} \tag{29}$$

$$\left[H^{j+1}\right]\begin{Bmatrix}\{u^{j+1}\}\\ \{u_{\mathrm{I}}^{j+1}\}\end{Bmatrix} = \{T^{j+1}\} \ , \ \left[H_{\mathrm{I}}^{j+1}\right]\begin{Bmatrix}\{u^{j+!}\}\\ \{u_{\mathrm{I}}^{j+1}\}\end{Bmatrix} = \left\{T_{\mathrm{I}}^{j+1}\right\} \tag{30}$$

where U^{j+1}, T^{j+1} and u^{j+1} denote the displacements, tractions, and the unknown variables of layer $j+1$ on the external surface, U_{I}^{j+1}, T_{I}^{j+1} and u_{I}^{j+1} the interface displacements, tractions, and the unknown variables of layer $j+1$ on the interface Γ_{I}.

We here suppose that the traction boundary conditions are prescribed on the external surfaces of Γ_j, and displacement boundary conditions are prescribed on the external surfaces of Γ_{j+1}. According to the equilibrium and compatibility conditions (25) and (26) at the interface, Eqs. (27)–(30) can be coupled as

$$\begin{bmatrix}\left[H^{j}\right] & [0]\\ \left[G_{\mathrm{I}}^{j}\right] & -\left[G_{\mathrm{I}}^{j+1}\right]\\ \left[H_{\mathrm{I}}^{j}\right] & \left[H_{\mathrm{I}}^{j+1}\right]\\ [0] & \left[G^{j+1}\right]\end{bmatrix}\begin{bmatrix}\begin{Bmatrix}\{u^{j}\}\\ \{u_{\mathrm{I}}^{j}\}\end{Bmatrix}\\ \begin{Bmatrix}\{u^{j+1}\}\\ \{u_{\mathrm{I}}^{j+1}\}\end{Bmatrix}\end{bmatrix} = \begin{bmatrix}\{T^{j}\}\\ \{0\}\\ \{0\}\\ \{U^{j+1}\}\end{bmatrix} \tag{31}$$

More equations will be added to this system in a similar way for other layers and the substrate. The system still needs to be reordered according to the prescribed displacement and traction boundary conditions.

4. Numerical results and discussions

To verify the methodologies developed above, three benchmark numerical examples are examined in which the proposed domain-decomposition GFDM solutions are compared with the corresponding exact solutions. In order to evaluate the performance of the numerical method, an L_2 error norm is defined as follows:

$$\textit{Global Error} = \left[\sum_{k=1}^{M}\left[I_{\mathrm{numer}}(k) - I_{exact}(k)\right]^{2}\right]^{1/2} \Big/ \left[\sum_{k=1}^{M}\left[I_{exact}(k)\right]^{2}\right]^{1/2}, \tag{32}$$

where $I_{\mathrm{numerical}}(k)$ and $I_{exact}(k)$ denote the numerical and analytical solutions at the kth calculated point, respectively, M is the number of calculation points tested. In our test cases, the simulated noisy data are generated using the following formula

$$\tilde{b} = b\left(1 + rand \times \frac{\delta}{100}\right), \tag{33}$$

where b is the exact boundary data, *rand* is a random number and its range is $-1 \le rand \le 1$, and δ stands for the level of noise.

4.1. Test problem 1: stress analysis in an amoeba-like domain

In order to validate the accuracy of the proposed GFDM model, we first consider the stress analysis in a single material with an irregular multiply-connected domain, as shown in Fig. 3. The computational domain with an irregular boundary $\partial\Omega = \Gamma_1 \cup \Gamma_2$ where Γ_1 is an amoeba-like domain defined by

$$\Gamma_1 = \left\{(r\cos\theta, r\sin\theta) : r = e^{\sin\theta}\sin^2(2\theta) + e^{\cos\theta}\cos^2(2\theta), 0 \le \theta \le 2\pi\right\}, \tag{34}$$

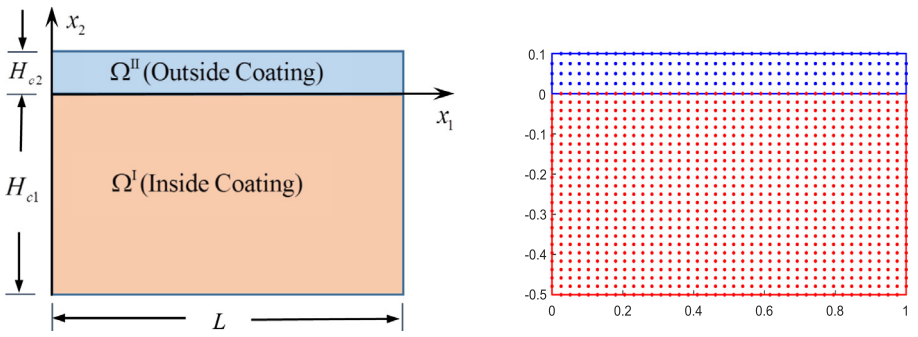

(a) Geometry of the problem (b) Configuration of the nodes distribution

Fig. 5. Geometry of the problem (a) and the configuration of the nodes distribution (b).

and the remaining boundary Γ_2 is a circle with radius $r=0.4$ and center at (0.5, 0.5). This 2D model is subjected to a mixed-type boundary condition, where the traction boundary conditions are prescribed on the outer surface of the domain and the displacement boundary conditions are imposed on the remaining surface.

For the ease of comparison, we consider the displacements with the following analytical solution

$$u_1(\boldsymbol{x}) = e^{x_1+x_2} + x_2, \quad u_2(\boldsymbol{x}) = \sin(x_1+x_2) + 1. \tag{35}$$

The elastic constants as introduced in Section 2 are taken to be $\mu=0.25$ (Poisson's ratio) and $E=200$ GPa (elastic modulus).

The relative error curves of the calculated stresses (σ_{11}, σ_{22} and σ_{12}) at interior points inside the whole computational domain are illustrated in Fig. 4, as functions of various number of GFDM nodes. As shown in Fig. 4, it can be seen that the proposed GFDM model is stable, accurate, and rapidly convergent as the number of nodes increases. It is also observed that the numerical results with only 700 collocation points are quite accurate for this 2D simulation. Although not presented here, it should be noted that analogous results have been obtained for displacements and stresses in the cases with other combinations of boundary conditions.

4.2. Test problem 2: a two-layered coating system on a rectangle

Next, we consider the stress analysis in a two-layered coating system, where $L=1m$ is the length of the system, $H_{c1}=0.5m$ the thickness of the inside coating, and $H_{c2}=0.1m$ the thickness of the outside coating. The geometric configuration of the problem and the GFDM nodes distribution are schematically shown in Fig. 5. This 2D model is subjected to a mixed-type boundary condition, where the tractions are prescribed on the external surfaces of the outside coating (Ω^{II}) and displacements are prescribed on the external surfaces of inside coating (Ω^{I}). Along the interface, the displacement and traction continuity conditions are given, see Eqs. (24) and (25). For this problem, we considered the solution of the Navier equations corresponding to the following exact solutions:

$$u_1(\boldsymbol{x}) = \cos(x_1+x_2) + \cos(x_2) + x_2, \quad u_2(\boldsymbol{x}) = \sin(x_1+x_2) + x_2 + 1, \tag{36}$$

for the outside coating, and

$$u_1(\boldsymbol{x}) = \cos(x_1+x_2) + \cos(x_2) + 1, \quad u_2(\boldsymbol{x}) = \sin(x_1+x_2) + \cos(x_2) + x_2, \tag{37}$$

for the inside coating. The elastic constants as introduced in Section 2 are taken to be $\mu=0.25$ (Poisson's ratio) and $E=200$ GPa (elastic modulus). For the numerical implementation, a total number of 1200 GFDM nodes are discretized inside the whole computational domain.

Figs. 6 and 7 illustrate the relative error curves of the calculated stresses and displacements at interior points along the coating-coating interface $x_2=0$. It can be seen that numerical results predicted by the proposed GFDM, for both stresses and displacements, are in excellent agreement with their corresponding analytical solutions, with the largest relative error less than 2E−4 for displacements and 3E−3 for stresses. It is also observed that the GFDM results with only 1200 nodes are quite accurate for this coating system, and the size of the resulting system of linear algebraic equations is quite small. In fact, for an i5-2.90 GHz computer, the total CPU times taken to solve this problem are 0.31 s for the proposed GFDM model.

Figs. 8 and 9 show the relative error curves of the computed displacements and stresses at interior points inside the whole computational

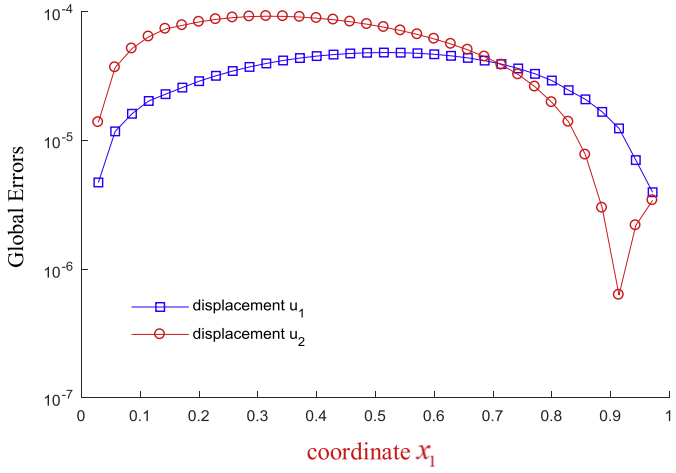

Fig. 6. Global error variation of the calculated displacements at points along the coating-coating interface ($x_2=0$).

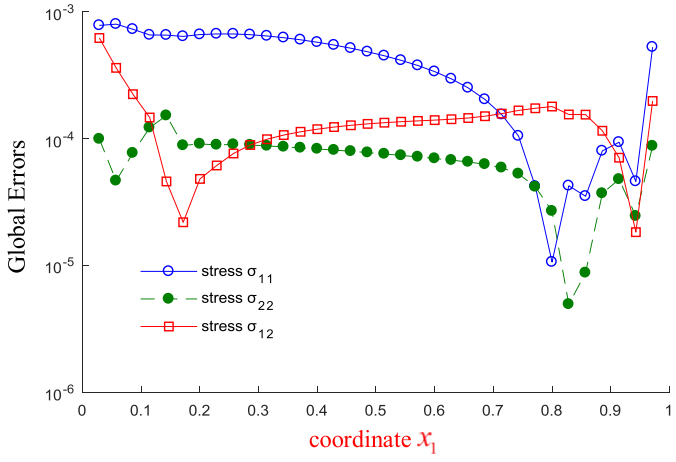

Fig. 7. Global error variation of the calculated stresses at points along the coating-coating interface ($x_2=0$).

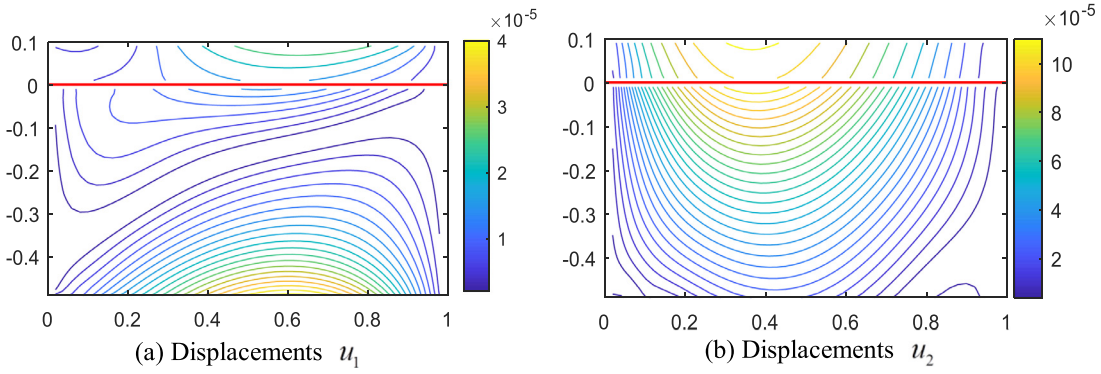

Fig. 8. Global error distribution for computed displacements at interior points inside the whole coating system.

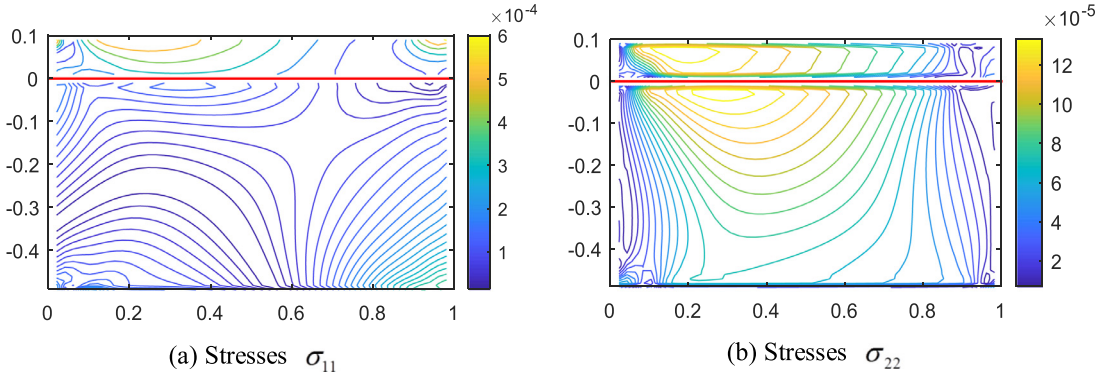

Fig. 9. Global error distribution for computed stresses at interior points inside the whole coating system.

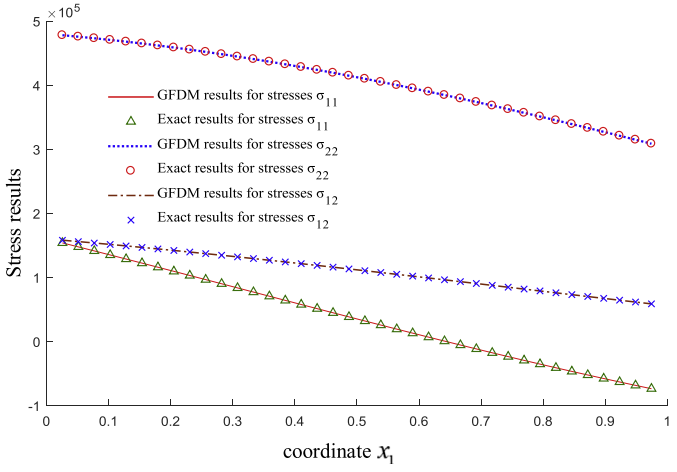

Fig. 10. Stress results calculated at points along the coating-coating interface ($x_2 = 0$).

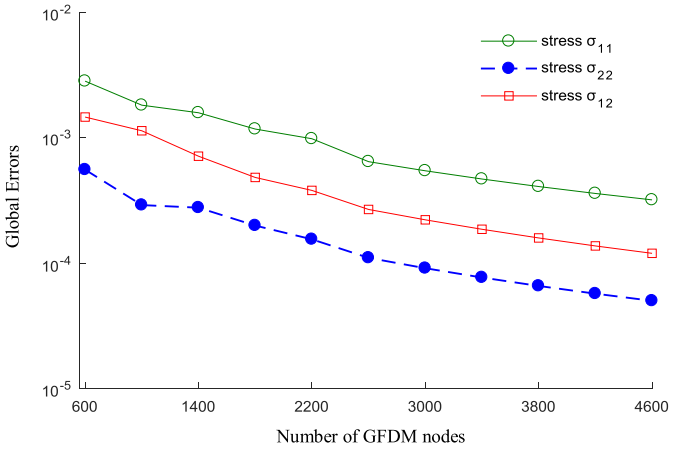

Fig. 11. Convergence curves of the calculated stresses at points inside the computational domain.

domain. As can be seen from these figures, the proposed GFDM scheme is extremely accurate for both displacements and stresses. In addition, stress results calculated at points along the coating–coating interface ($x_2 = 0$) are listed in Fig. 10. The relative error curves of the calculated stresses (σ_{11}, σ_{22} and σ_{12}) at interior points inside the whole computational domain are illustrated in Fig. 11, as functions of various number of GFDM nodes. As shown in Fig. 11, it can be seen that the proposed GFDM model is stable, accurate, and rapidly convergent as the number of nodes increases. We can also observed that the convergence rate for both stresses is about 1.65. We can conclude that the GFDM, in conjunction with the domain decomposition technique, can provide stable and accurate numerical solutions for multi-layered elastic problems.

4.3. Test problem 3: a circular shaft with two layers of coatings

Finally, a circular shaft with two layers of coating is considered, as shown in Fig. 12. The layers of coatings consist of different materials (Young's modulus of outside coating/Young's modulus of inner coating = 1/2 and Poisson ratio of outside coating = Poisson ratio of inner coating = 0.2). The shaft and the two coatings have outer radii $r_1 = 5m$, $r_2 = 6m$ and $r_3 = 7m$, respectively. It is assumed that the coatings are free to expand laterally except at the interface to the rigid shaft, but are

Table 1
Radial and tangential stress results calculated at point A by using different GFDM node number.

GFDM nodes	Radial stress σ_r			Tangential stress σ_θ		
	Exact solutions	GFDM solutions	Relative errors	Exact solutions	GFDM solutions	Relative errors
1000	−1.0496	−1.0430	6.2156E−3	−0.4995	−0.4991	8.2156E−4
2000		−1.0479	1.5622E−3		−0.4994	2.5125E−4

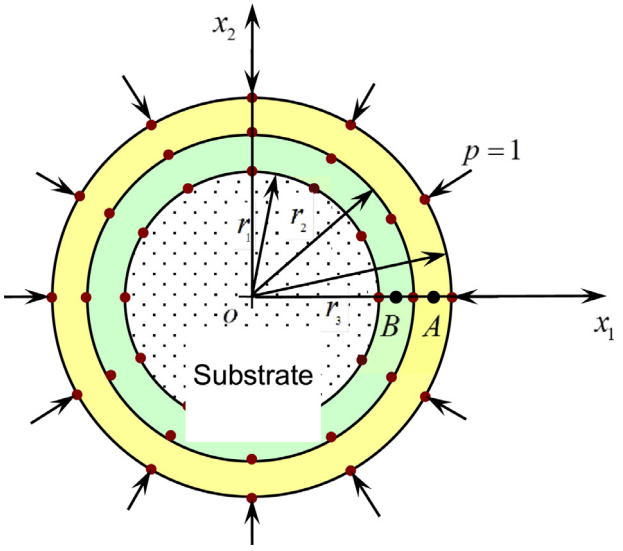

Fig. 12. Cross-section of a shaft with two layers of coatings.

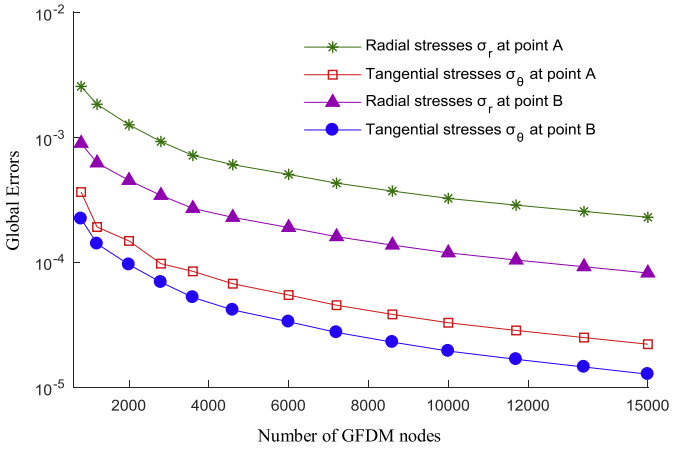

Fig. 13. Convergence curves of the calculated radial and tangential stresses at interior point *A* and *B*.

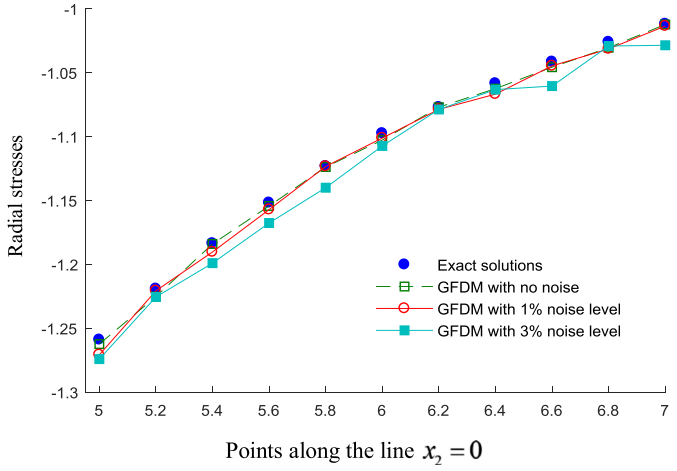

Fig. 14. Analytical and GFDM results of radial stress (σ_r) solutions calculated at points along the line $x_2=0$.

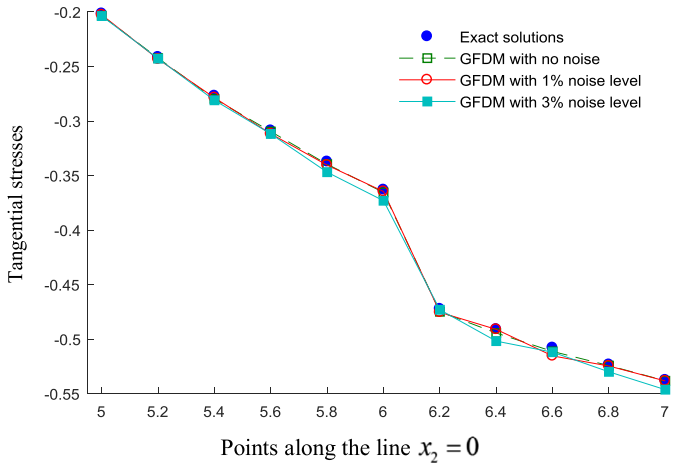

Fig. 15. Analytical and GFDM results of tangential stress (σ_θ) solutions calculated at points along the line $x_2=0$.

constrained axially so that a condition of plane strain relative to x_1-x_2 plane exists. Also it is assumed that the coating system is loaded by a uniform pressure $p=1$ which is distributed around the circumference of the outside coating. The boundary conditions for the displacement, considering the rigid shaft assumption, are $u_r=u_\theta=0$ for all nodes at the shaft-coating interface, where (r, θ) denotes the polar coordinates. The analytical solutions corresponding to this coating system can be found in Ref. [53].

To investigate the convergence of the proposed method, the relative error curves of the calculated radial (σ_r) and tangential (σ_θ) stresses at interior points A(5.5, 0) and B(6.5, 0) are illustrated in Fig. 13, as functions of various number of GFDM nodes. As shown in Fig. 13, both the GFDM results converge towards their corresponding analytical solutions as the number of nodes increases. It can be also seen from Fig. 13 that the global errors decrease until the number of GFDM nodes reaches the value $N=10,000$, after which a further increase in the number of nodes does not improve substantially the accuracy of the numerical results.

Next, we examine the sensitivity of the GFDM results with respect to various levels of noise added into the input data. The GFDM results for radial (σ_r) and tangential (σ_θ) stresses at interior points on the line $x_2=0$, computed using exact, 1% and 3% noise added into the input data, are illustrated in Figs. 14 and 15, respectively. As shown in these figures, the GFDM solutions retrieved for both σ_r and σ_θ are in good agreement with their corresponding exact solutions, even with a relatively large amount of noise (3%) added into the input data. It is also shown that, as expected, the GFDM solutions converge to their corresponding exact solutions as the amount of noise decreases. In addition, radial and tangential stress results calculated at point A are illustrated in Table 1. Similar results have been obtained also for the other components of the displacements and stresses analyzed, but they are not presented here for the sake of brevity.

5. Concluding remarks

In this study, we demonstrate the applicability of the generalized finite difference method (GFDM) for the stress analysis in multi-layered elastic materials. The multi-layered problems under consideration are solved using a domain decomposition technique, in which the composite material is decomposed into several sub-domains and, in each subdomain, the solution is approximated by using the GFDM-type expansion. On the subdomain interface, compatibility of displacements and equilibrium of tractions are imposed. These interface continuity conditions are satisfied in a least-squares sense in the same way as the boundary conditions of the problem. Three benchmark numerical examples clearly demonstrate the stability and accuracy of the proposed GFDM scheme. However, further analyses and optimized implementation are required in order to fully explore the efficiency and accuracy of the new method. These include the detailed convergence order analyses of the method, optimized strategies for adaptive nodes refinements, as well as the optimal choice of many different parameters. Results along these lines will be presented in the future.

Acknowledgments

The work described in this paper was supported by the National Natural Science Foundation of China (Nos. 11402075, 11401332 and 71571108), Projects of International (Regional) Cooperation and Exchanges of NSFC (No. 71611530712), and the Natural Science Foundation of Shandong Province of China (Nos. ZR2017BA003, ZR2015GZ007 and ZR2017JL004).

References

[1] Karageorghis A, Lesnic D. Steady-state nonlinear heat conduction in composite materials using the method of fundamental solutions. Comput Methods Appl Mech Eng 2008;197(33-40):3122–37.
[2] Yao ZH, Xu JD, Wang HT, Zheng XP. Simulation of CNT composites using fast multipole BEM. J Mar Sci Technol 2009;17(3):194–202.
[3] Tomas Johansson B, Lesnic D. A method of fundamental solutions for transient heat conduction in layered materials. Eng Anal Bound Elem 2009;33(12):1362–7.
[4] Gu Y, Chen W, Zhang C. Stress analysis for thin multilayered coating systems using a sinh transformed boundary element method. Int J Solids Struct 2013;50(20–21):3460–71.
[5] Xie G, Zhou F, Zhang J, Zheng X, Huang C. New variable transformations for evaluating nearly singular integrals in 3D boundary element method. Eng Anal Bound Elem 2013;37(9):1169–78.
[6] Gu Y, He X, Chen W, Zhang C. Analysis of three-dimensional anisotropic heat conduction problems on thin domains using an advanced boundary element method. Comput Math Appl 2018;75(1):33–44.
[7] Qu W, Chen W, Gu Y. Fast multipole accelerated singular boundary method for the 3D Helmholtz equation in low frequency regime. Comput Math Appl 2015;70(4):679–90.
[8] Liu YJ. A fast multipole boundary element method for 2D multi-domain elastostatic problems based on a dual BIE formulation. Comput Mech 2008;42(5):761–73.
[9] Cheng AHD, Cheng DT. Heritage and early history of the boundary element method. Eng Anal Bound Elem 2005;29(3):268–302.
[10] Basar Y, Ding Y. Finite-element analysis of hyperelastic thin shells with large strains. Comput Mech 1996;18(3):200–14.
[11] Gu Y, Gao H, Chen W, Zhang C. A general algorithm for evaluating nearly singular integrals in anisotropic three-dimensional boundary element analysis. Comput Methods Appl Mech Eng 2016;308:483–98.
[12] Chen CS, Ganesh M, Golberg MA, Cheng AHD. Multilevel compact radial functions based computational schemes for some elliptic problems. Comput Math Appl 2002;43(3–5):359–78.
[13] Lin J, Zhang C, Sun L, Lu J. Simulation of seismic wave scattering by embedded cavities in an elastic half-plane using the novel singular boundary method. Adv Appl Math Mech 2018;10:322–42.
[14] Li J, Fu Z, Chen W. Numerical investigation on the obliquely incident water wave passing through the submerged breakwater by singular boundary method. Comput Math Appl 2016;71(1):381–90.
[15] Wang F, Chen W, Zhang C, Lin J. Analytical evaluation of the origin intensity factor of time-dependent diffusion fundamental solution for a matrix-free singular boundary method formulation. Appl Math Model 2017;49:647–62.
[16] Chen CS, Cho HA, Golberg MA. Some comments on the ill-conditioning of the method of fundamental solutions. Eng Anal Bound Elem 2006;30(5):405–10.
[17] Sarler B. Solution of potential flow problems by the modified method of fundamental solutions: formulations with the single layer and the double layer fundamental solutions. Eng Anal Bound Elem 2009;33(12):1374–82.
[18] Chen W, Gu Y. An improved formulation of singular boundary method. Adv Appl Math Mech 2012;4(5):543–58.
[19] Qu W, Chen W. Solution of two-dimensional stokes flow problems using improved singular boundary method. Adv Appl Math Mech 2015;7(1):13–30.
[20] Fu Z-J, Chen W, Yang H-T. Boundary particle method for Laplace transformed time fractional diffusion equations. J Comput Phys 2013;235(Supplement C):52–66.
[21] Liu GR, Nguyen-Thoi T, Nguyen-Xuan H, Lam KY. A node-based smoothed finite element method (NS-FEM) for upper bound solutions to solid mechanics problems. Comput Struct 2009;87(1–2):14–26.
[22] Marin L. A meshless method for the stable solution of singular inverse problems for two-dimensional Helmholtz-type equations. Eng Anal Bound Elem 2010;34(3):274–88.
[23] Sarler B, Vertnik R. Meshfree explicit local radial basis function collocation method for diffusion problems. Comput Math Appl 2006;51(8):1269–82.
[24] Nguyen VP, Rabczuk T, Bordas S, Duflot M. Meshless methods: a review and computer implementation aspects. Math Comput Simul 2008;79(3):763–813.
[25] Gu Y, Chen W, Gao H, Zhang C. A meshless singular boundary method for three-dimensional elasticity problems. Int J Numer Methods Eng 2016;107(2):109–26.
[26] Liszka T. An interpolation method for an irregular net of nodes. Int J Numer Methods Eng 1984;20(9):1599–612.
[27] Liszka T, Orkisz J. The finite difference method at arbitrary irregular grids and its application in applied mechanics. Comput Struct 1980;11(1):83–95.
[28] Payre GMJ. Influence graphs and the generalized finite difference method. Comput Methods Appl Mech Eng 2007;196(13–16):1933–45.
[29] Ureña F, Benito JJ, Salete E, Gavete L. A note on the application of the generalized finite difference method to seismic wave propagation in 2D. J Comput Appl Math 2012;236(12):3016–25.
[30] Benito JJ, Urena F, Gavete L. Influence of several factors in the generalized finite difference method. Appl Math Model 2001;25(12):1039–53.
[31] Gu Y, Wang L, Chen W, Zhang C, He X. Application of the meshless generalized finite difference method to inverse heat source problems. Int J Heat Mass Transf 2017;108(Part A):721–9.
[32] Shu C, Ding H, Yeo KS. Local radial basis function-based differential quadrature method and its application to solve two-dimensional incompressible Navier–Stokes equations. Comput Methods Appl Mech Eng 2003;192(7):941–54.
[33] Tolstykh AI, Shirobokov DA. On using radial basis functions in a “finite difference mode” with applications to elasticity problems. Comput Mech 2003;33(1):68–79.
[34] Shan YY, Shu C, Qin N. Multiquadric finite difference (MQ-FD) method and its application. Adv Appl Math Mech 2009;1(5):615–38.
[35] Roque CMC, Cunha D, Shu C, Ferreira AJM. A local radial basis functions—finite differences technique for the analysis of composite plates. Eng Anal Bound Elem 2011;35(3):363–74.
[36] Hidayat MIP, Wahjoedi BA, Parman S, Megat Yusoff PSM. Meshless local B-spline-FD method and its application for 2D heat conduction problems with spatially varying thermal conductivity. Appl Math Comput 2014;242:236–54.
[37] Dehghan M, Abbaszadeh M. The meshless local collocation method for solving multi--dimensional Cahn-Hilliard, Swift-Hohenberg and phase field crystal equations. Eng Anal Bound Elem 2017;78:49–64.
[38] Gavete L, Gavete ML, Benito JJ. Improvements of generalized finite difference method and comparison with other meshless method. Appl Math Model 2003;27(10):831–47.
[39] Hua Q, Gu Y, Qu W, Chen W, Zhang C. A meshless generalized finite difference method for inverse Cauchy problems associated with three-dimensional inhomogeneous Helmholtz-type equations. Eng Anal Bound Elem 2017;82:162–71.
[40] Ureña F, Salete E, Benito JJ, Gavete L. Solving third- and fourth-order partial differential equations using GFDM: application to solve problems of plates. Int J Comput Math 2012;89(3):366–76.
[41] Gavete L, Urena F, Benito JJ, Salete E. A note on the dynamic analysis using the generalized finite difference method. J Comput Appl Math 2013;252:132–47.
[42] Gavete L, Ureña F, Benito JJ, García A, Ureña M, Salete E. Solving second order non-linear elliptic partial differential equations using generalized finite difference method. J Comput Appl Math 2017;318:378–87.
[43] Fan CM, Huang YK, Li PW, Chiu CL. Application of the generlized finite-difference method to inverse biharmonic boundary-value problems. Numer Heat Tranf B – Fundam 2014;65(2):129–54.
[44] Gu Y, Lei J, Fan C-M, He X-Q. The generalized finite difference method for an inverse time-dependent source problem associated with three-dimensional heat equation. Eng Anal Bound Elem 2018;91:73–81.
[45] Belytschko T, Krongauz Y, Organ D, Fleming M, Krysl P. Meshless methods: an overview and recent developments. Comput Methods Appl Mech Eng 1996;139(1):3–47.
[46] Liu GR, Gu YT. A local radial point interpolation method (LRPIM) for free vibration analysis of 2-D solids. J Sound Vib 2001;246(1):29–46.
[47] Abbasbandy S, Shirzadi A. MLPG method for two-dimensional diffusion equation with Neumann’s and non-classical boundary conditions. Appl Numer Math 2011;61(2):170–80.
[48] Gu YT, Liu GR. A boundary point interpolation method for stress analysis of solids. Comput Mech 2002;28(1):47–54.
[49] Karageorghis A, Lesnic D, Marin L. A survey of applications of the MFS to inverse problems. Inverse Probl Sci Eng 2011;19(3):309–36.
[50] Lee S-C, Vouvakis MN, Lee J-F. A non-overlapping domain decomposition method with non-matching grids for modeling large finite antenna arrays. J Comput Phys 2005;203(1):1–21.
[51] Lube G, Müller L, Otto FC. A non-overlapping domain decomposition method for the advection-diffusion problem. Computing 2000;64(1):49–68.

[52] Berger JR, Karageorghis A. The method of fundamental solutions for layered elastic materials. Eng Anal Bound Elem 2001;25(10):877–86.
[53] Gu Y, Chen W, He XQ. Domain-decomposition singular boundary method for stress analysis in multi-layered elastic materials. Comput Mater Contin 2012;29(2):129–54.
[54] Yan Z, Wei C, Zhang C. Band structures of elastic SH waves in nanoscale multi-layered functionally graded phononic crystals with/without nonlocal interface imperfections by using a local RBF collocation method. Acta Mech Solida Sin 2017;30(4):390–403.
[55] Gavete L, Benito JJ, Ureña F. Generalized finite differences for solving 3D elliptic and parabolic equations. Appl Math Model 2016;40(2):955–65.
[56] Fan CM, Li PW, Yeih WC. Generalized finite difference method for solving two-dimensional inverse Cauchy problems. Inverse Probl Sci Eng 2015;23(5):737–59.
[57] Gao XW, Guo L, Zhang C. Three-step multi-domain BEM solver for nonhomogeneous material problems. Eng Anal Bound Elem 2007;31(12):965–73.